Cerenkov Luminescence Imaging in Prostate Cancer: Not the Only Light That Shines

Judith olde Heuvel[1,2], Berlinda J. de Wit-van der Veen[1], Henk G. van der Poel[3], Pim J. van Leeuwen[3], Elise M. Bekers[4], Maarten R. Grootendorst[5], Kunal N. Vyas[5], Cornelis H. Slump[2], and Marcel P.M. Stokkel[1]

[1]Department of Nuclear Medicine, Netherlands Cancer Institute, Amsterdam, The Netherlands; [2]Technical Medical Centre, University of Twente, Enschede, The Netherlands; [3]Department of Urology, Netherlands Cancer Institute, Amsterdam, The Netherlands; [4]Department of Pathology, Netherlands Cancer Institute, Amsterdam, The Netherlands; and [5]Lightpoint Medical Ltd., Chesham, United Kingdom

Cerenkov luminescence imaging (CLI) is a novel imaging technology that might have the ability to assess surgical margins intraoperatively during prostatectomy using ^{68}Ga-prostate-specific membrane antigen (^{68}Ga-PSMA-11). This study evaluated the accuracy of CLI compared with histopathology and, as an exploratory objective, investigated the characteristics of the identified chemiluminescence signal. **Methods:** After intravenous injection of a mean ^{68}Ga-PSMA-11 activity of 69 MBq intraoperatively, all excised specimens were imaged with CLI. Areas of increased signal were marked for histopathologic comparison and scored for the likelihood of being a positive surgical margin (PSM) using a 5-point Likert scale. In addition, the chemiluminescence signal was investigated in 3 radioactive and 3 nonradioactive specimens using CLI. **Results:** In 15 patients, the agreement between CLI and histopathology was 60%; this improved to 83% when including close surgical margins (≤1 mm). In 6 hot spots, CLI correctly identified PSMs on histopathology, located at the apex and mid prostate. In all 15 patients, an increased signal at the prostate base was observed, without the presence of the primary tumor in this area in 8 patients. This chemiluminescence signal was also observed in nonradioactive prostate specimens, with a half-life of 48 ± 11 min. The chemiluminescence hampered the visual interpretation of 4 PSMs at the base. **Conclusion:** CLI was able to correctly identify margin status, including close margins, in 83% of the cases. The presence of a diathermy-induced chemiluminescent signal hampered image interpretation, especially at the base of the prostate. In the current form, CLI is most applicable to detect PSMs and close margins in the apex and mid prostate.

Key Words: Cerenkov luminescence imaging; prostate cancer; ^{68}Ga-PSMA; intraoperative assessment; surgical margins

J Nucl Med 2022; 63:29–35
DOI: 10.2967/jnumed.120.260034

Positive surgical margins (PSMs) on histopathology occur in 11%–38% of the patients undergoing a radical prostatectomy (*1*,*2*). These men have a higher risk of receiving adjuvant local radiotherapy (*1*,*3*). Multiple intraoperative technologies for margin assessment are being developed that aim to enable a radical excision (*4*). Of these, neurovascular structure-adjacent frozen-section examination (NeuroSAFE) is currently the only method used for clinical decision making with good diagnostic accuracy (sensitivity, 93.5%; specificity, 98.8%) (*5*), but the procedure is labor-intensive, time-consuming, and costly and is prone to sampling errors and therefore used in only a few centers (*6*). In addition, a study showed that 70% of the secondary resections due to a PSM on NeuroSAFE did not contain tumor (*7*).

A recently introduced technology to aid intraoperative margin assessment is Cerenkov luminescence imaging (CLI) (*8*–*12*). Cerenkov radiation is induced when a charged particle travels more quickly than the velocity of light in the tissue, thus polarizing the tissue. When the locally polarized medium returns to its ground state, Cerenkov photons are emitted (*10*). Tumor-specific tracers, such as ^{68}Ga-prostate-specific membrane antigen (^{68}Ga-PSMA-11), induce Cerenkov radiation, and the detected rays from superficial layers can guide toward areas in which a PSM is highly suspected. Recent studies on this application have already shown its feasibility and safety (*13*,*14*).

During radical prostatectomy, electrosurgery (i.e., diathermy) is used for cutting and coagulation of tissue. This technique uses radiofrequency currents to increase the intracellular temperature, which in turn can result in vaporization and blood clotting. A preclinical study suggested that heat may induce chemiluminescence with wavelengths of between 400 and 710 nm (*15*,*16*), which overlap with the Cerenkov spectrum (400–1,000 nm) (*9*). Thus, this chemiluminescence might interfere with the CLI signal, indicating a potential limitation (*15*,*16*). However, these studies were conducted with animal tissue and used other thermal sources; thus, the spectrum, half-life, and other features in human perfused tissue after diathermy application are unknown.

In our prior study, the technical feasibility of ^{68}Ga-PSMA-11 CLI for margin assessment was assessed in a small population with prostate cancer (*14*). This consecutive study evaluated the accuracy of CLI compared with histopathology in a larger population and, as an explorative objective, investigated the characteristics of the chemiluminescent signal observed on CLI.

MATERIALS AND METHODS

The present study was approved by the local Ethics Committee (NL8256, https://www.trialregister.nl/), and all subjects gave written informed consent. High-risk primary prostate cancer patients scheduled for robot-assisted radical prostatectomy were enrolled. The inclusion criteria were biopsy-proven prostate cancer with a tumor lesion of at least 1.5 cm on MRI and a PSMA-positive intraprostatic lesion on

Received Nov. 27, 2020; revision accepted Apr. 1, 2021.
For correspondence or reprints, contact B.J. de Wit-van der Veen (l.vd.veen@nki.nl).
Published online Apr. 30, 2021.

PSMA PET/CT (^{18}F-DCFPyL or ^{68}Ga-PSMA-11). The exclusion criterion was the use of indocyanine green during surgery (not standard of care), since this may influence CLI measurements. In all patients, CLI was not used for surgical or histopathologic decision making.

Surgery and Intraoperative CLI

An intravenous injection of approximately 100 MBq of ^{68}Ga-HBED-CC-PSMA (ABX GmbH) was given after docking the daVinci surgical system. Immediately after prostatectomy, ex vivo Cerenkov images of the prostate specimen were acquired with the LightPath system (Lightpoint Medical Ltd.) using the following imaging parameters: exposure time of 150 s, 8 × 8 pixel binning (pixel resolution, 938 μm), and no optical filter. A 550-nm short-pass filter was applied when areas of increased signal (called hot spots) were visualized on nonfiltered images.

Understanding the Characteristics of the Chemiluminescent Signal

Effect of Urine Contamination on CLI. Since ^{68}Ga-PSMA-11 undergoes renal clearance, we verified whether radioactive urine might affect CLI by first imaging 3 specimens without rinsing of potential blood and urine contamination. Subsequently, the specimens were rinsed twice with 500 mL of 0.9% NaCl and imaged again. The visual and quantitative differences between the images were compared. In the other patients, CLI was performed after rinsing the prostate once with 500 mL of 0.9% NaCl.

CLI and Flexible Autoradiography (FAR) of Nonradioactive Prostate Specimens. The prostate specimens of 3 patients undergoing prostatectomy without injection of ^{68}Ga-PSMA-11 (the nonradioactive specimens) were imaged with CLI to investigate the characteristics of the chemiluminescence signal. On these images, multiple regions of interest were drawn to quantify any chemiluminescence signal and the reduction in this signal by applying a 550-nm short-pass filter (application of 800-nm short-pass filter is shown in Supplemental Fig. 1; supplemental materials are available at http://jnm.snmjournals.org). The half-life of chemiluminescence was determined by consecutive imaging over approximately 60 min.

To investigate an alternative imaging method that is potentially less susceptible to chemiluminescence than CLI, FAR was used on nonradioactive specimens. A 12-μm flexible scintillating film (Lightpoint Medical Ltd. and Scintacor Ltd.) was draped over the specimen, and as a whole this was imaged within the LightPath system, thus obviating development of a scintillating film. The opaque nature of the scintillator may block some of the chemiluminescent photons while detecting the positrons emitted by ^{68}Ga-PSMA-11 (*17*). The reduction in chemiluminescent signal from photon absorption by the FAR was assessed, as well as the half-life over an approximately 60-min measurement period.

FAR on ^{68}Ga-PSMA-11–Containing Prostate Specimens. In 3 CLI patients, FAR was used in addition to CLI imaging on ^{68}Ga-PSMA-11–containing prostate specimens. Images with and without a 550-nm short-pass filter were acquired to investigate the effect of FAR on the signal originating from ^{68}Ga-PSMA-11 uptake and in relation to chemiluminescence.

Histopathology

After CLI acquisitions, the specimens were sent for standard histopathologic examination by an experienced uropathologist. A PSM was defined as cancer extending into the inked surface in accordance with the guidelines (*18*). At the marked locations, the tumor–to–specimen edge distance was measured.

Image Analysis

Images were quantified and processed in MATLAB, version R2017b (The MathWorks), as previously described (*14*). The mean radiance (photons/s/cm^2/steradian) was measured in areas showing hot spots (suspected tumor) and in areas with no increased signal (tissue background), and the signal-to-tissue background ratios (SBRs) were calculated. Hot spots were defined as all signals higher than 3 times the SD of the empty background (*19*). Visual interpretation of all images was performed postoperatively by 2 independent readers. To assess the likelihood that such a hot spot was actually a PSM, all hot spots were scored using a 5-point Likert scale (LS) (1 being most likely a negative surgical margin [NSM] and 5 being most likely a PSM). Features used to interpret hot spots were knowledge of the tumor location on PSMA PET/CT, size of the hot spot (required size ≥ 1 mm due to 8 × 8 binning), intensity above the tissue background level, and use of diathermy. Observers were masked to each other's scores and to histopathology findings; any disagreement was settled by consensus. A score on the LS of 4 or 5 was considered PSM in further analysis; 1–3 was considered NSM. The extent of the PSMs was measured on CLI images (longest axis) and compared with the extent measured on histopathology. Agreement between the margin status on histopathology and on CLI was assessed in 3 areas of the prostate: base (top 1 cm), mid gland, and apex (bottom 1 cm). Agreement was calculated with and without additional scoring (using the LS) and with and without inclusion of a close surgical margin (CSM, ≤1-mm tumor–to–specimen edge distance).

RESULTS

Intraoperative CLI Radioactive Specimens

In this study, 17 patients were included. One patient had to be excluded because of an unsuccessful ^{68}Ga-PSMA-11 labeling on the day of the surgery, and another was excluded because of the use of indocyanine green, leaving 15 patients in the analysis. The mean injected activity (±SD) was 69 ± 27 MBq (range, 23–121 MBq), with an average of 70 ± 15 min (range, 44–105 min) between injection and CLI acquisition. The patient and procedure characteristics can be found in Table 1.

Figure 1 displays examples of CLI images showing hot spots identified as PSM, NSM, or CSM on histopathology. The overall agreement between CLI (hot spot) and histopathology with respect to the margin status (PSM or NSM) was 31% without further Likert scoring by users (Fig. 2; Supplemental Table 1). This overall agreement improved to 59% when margins of 1 mm or less (CSM) on histopathology were also classified as positive. CLI and histopathology were discordant mainly at the prostate base.

Additionally, all hot spots on CLI were interpreted using the 5-point LS by the independent users. Disagreement between readers occurred in 8 hot spots, and concordance was reached by consensus. In all these cases, the disagreement concerned 4 versus 5, or 1 versus 2–3. With the addition of the LS, overall agreement between CLI and histopathology was 60%, which improved to 83% with inclusion of CSM. Ten hot spots were identified as histopathologically confirmed PSMs (Table 2); 6 were at the apex or mid prostate, with an LS of at least 4 (true-positive), and 4 were at the base, with an LS of 3 (false-negative). There were no proven PSMs that did not show a signal on CLI. The extent of PSMs measured on CLI and histopathology differed by less than 1 mm in 5 of 10 instances (Table 2).

The average SBR was 7.1 ± 3.5 for PSM, 5.0 ± 1.9 for CSM, and 5.8 ± 3.9 for NSM on a nonfiltered image (Fig. 3).

In all 15 patients, an intense signal was observed on CLI at the prostate base (Fig. 3). In 8 of these patients, the tumor was not in the base, as indicated on preoperative PET/CT. These findings

TABLE 1
Patient Demographics, TNM Classification, Tumor Characteristics, TBR on Preoperative PET/CT Scan, and Information Regarding CLI Imaging

Patient no.	Age (y)	Preoperative TNM	Postoperative TNM	PSA (μg/L)	Gleason score, preoperative biopsy	TBR on PSMA PET	Intraoperative injected activity (MBq)	Time between injection and CLI imaging (h:min)	Estimated* activity in prostate at start of CLI imaging (kBq)
1	67	cT3bN0M0	pT3aN0R1	29.9	4 + 4 = 8	4.9	118.0	01:35	111
2	71	cT2bN0M0	pT3aN0R1	4.4	4 + 4 = 8	8.1	68.4	01:04	93
3	58	cT1cN0M0	pT2cN0R0	5.3	4 + 4 = 8	1.8	88.1	01:25	26
4	73	cT3bN1M0	pT3bN1R0	8.3	4 + 5 = 9	8.9	75.6	00:59	92
5	66	cT3bN0M0	pT3bN0R0	2.7	4 + 4 = 8	2.1	96.7	01:00	52
6	63	cT2aN0M0	pT2N0R0	6.4	4 + 5 = 9	3.8	64.6	01:02	37
7	55	cT2cN0M0	pT3aN1R0	9.3	4 + 4 = 8	3.7	62.1	01:14	61
8	48	cT3bN1M0	pT3bN1R1	4.4	4 + 5 = 9	4.4	23.4	01:05	48
9	73	cT2cN0M0	PT3aN0R0	5.6	4 + 3 = 7	2.7	44.7	00:44	26
10	69	cT3aN0M0	pT3aN0R1	65	4 + 5 = 9	2.4	47.9	00:56	151
11	72	cT2bN0M0	pT3bN1R0	8.7	4 + 4 = 8	2.8	47.6	01:05	42
12	76	cT1cN0M0	pT2N0R1	9.2	3 + 4 = 7	2.5	65.4	01:02	69
13	65	cT2cN0M0	pT3aN0R1	5.1	4 + 3 = 7	1.7	121.1	01:26	8
14	67	cT2bN0M0	pT3bN0R1	18.6	4 + 5 = 9	3.7	37.4	01:14	14
15	74	cT1cN0M0	pT2cN0R0	7.9	4 + 4 = 8	3.5	70.2	01:45	33

*Based on uptake on preoperative PET imaging (uptake in prostate as percentage injected activity).
PSA = prostate-specific antigen; TBR = tumor-to-background ratio.

indicate the presence of an additional chemiluminescence signal, which may explain the high false-negative rate at the base.

Understanding the Characteristics of the Chemiluminescent Signal

Effect of Urine Contamination on CLI. After rinsing once, the chemiluminescence signal at the base was reduced to 93% of the original CLI signal (Supplemental Fig. 2). After the second rinsing, the signal decreased to 88% compared with the unrinsed prostate. The time between the rinsed and unrinsed images was, respectively, 5 and 10 min for the first and second rinsings.

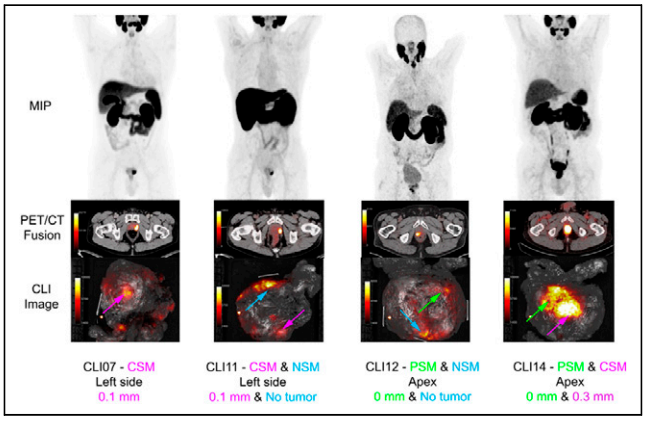

FIGURE 1. Examples of PET/CT and CLI images from 4 patients: maximum-intensity projections (MIPs) of preoperative PSMA PET, transversal PET/CT images at height of primary tumor, and CLI images of excised prostate specimens without optical filter. Arrows locate hot-spot areas; green, PSM; blue, NSM; and pink, CSM with tumor ≤ 1 mm from margin, according to pathologist. Corresponding tumor–to–specimen edge distances on histopathology are noted below images.

CLI and FAR of Nonradioactive Prostate Specimens. The chemiluminescent signal was also visible on CLI images from 3 nonradioactive specimens, primarily at the base (Fig. 4). This observation underlines the hypothesis that chemiluminescence does not originate from ^{68}Ga-PSMA-11. The SBR of the chemiluminescence was 4.9 ± 1.1 on the unfiltered image. The half-life was 48 ± 11 min without an optical filter and 52 ± 16 min with the 550-nm filter. The application of a 550-nm short-pass filter resulted in a reduction to 15% of the original chemiluminescence signal, which was comparable to the CLI signal reduction by filtering in radioactive specimens (18%). The application of FAR reduced the chemiluminescent signal to 60% of the original CLI image, both with and without 550-nm filtering (Fig. 5).

FAR on ^{68}Ga-PSMA-11–Containing Prostate Specimens. FAR of the radioactive specimens reduced the chemiluminescence to 70% at locations where diathermy was applied, whereas tumor and tissue background signals were amplified by FAR to, on average, 3.2 times the original signal (Fig. 5; Supplemental Fig. 3).

DISCUSSION

The primary aim of the current study was to assess the concordance in margin status between intraoperative CLI and postoperative histopathology. This study showed that agreement between CLI and histopathology ranged from 31% to 83% depending on definition of PSM and addition of image interpretation by LS. The explorative aim of the study was to characterize the observed chemiluminescence. This signal was found to be unrelated to ^{68}Ga-PSMA-11, to have a mean SBR of 4.9 ± 1.1, and to have a

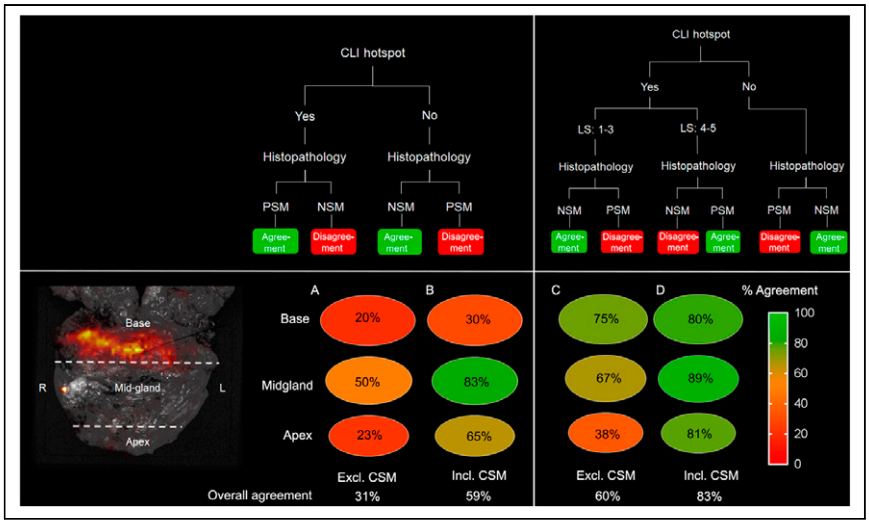

FIGURE 2. Agreement between CLI and histopathology in all patients divided into 3 regions of prostate. (A) Agreement between CLI hot spot (yes or no) and histopathology (PSM or NSM), excluding CSM. (B) Agreement including CSM (≤1 mm). (C) Agreement when adding LS to CLI hot spot. (D) Agreement with LS, including CSM. Overall agreement is noted below circles. Excl. = excluding; incl. = including.

half-life of 48 ± 11 min. This chemiluminescence indeed proved clinically relevant as it hampered easy identification of 4 of 10 PSMs on CLI, all 4 located at the base.

When the histopathologic PSM definition is considered as tumor on ink, the false-positive rate found in the current study can be considered high, with 24 of 30 hot spots (LS ≥ 4) not having a PSM on histopathology (agreement, 31%). Comparable false-positive rates were also described by Darr et al., though their workflow and CLI protocol were slightly different (*13*). Several explanations for these false-positives findings can be considered. First, in 19 false-positives, the tumor–to–specimen edge distance was within 1 mm on histopathology. Because of the average positron range of 2.8 mm for ^{68}Ga (*20*), the CLI technique has inherent difficulties in the detection of PSMs defined as tumor on ink. If instead of tumor on ink a PSM is defined as a margin of 1 mm or less, agreement between CLI and histopathology increases to 83%. The clinical relevance of a CSM is a matter of debate; some argue that compared with an NSM, a CSM results in a higher rate of biochemical recurrence, though it is not an independent predictor (*21*). A CSM was found to have a role in biochemical recurrence by Izard et al. as well, though those investigators defined a CSM as being less than 0.1 mm (*22*). CLI might have added value in guiding surgeons toward areas with an increased risk on PSMs and CSMs. The positron range might also influence the correlation between the extent of the PSM on CLI and histopathology; in 5 of 10 PSMs, the deviation between the extent on CLI and histopathology was more than 1 mm (Table 2). This difference can also be caused by shrinkage of the specimen during fixation and histopathologic processing. Still, it is worth further exploring, as the extent of a PSM is an important prognostic factor (*23*).

Second, the presence of the chemiluminescence signal also contributed to the false-positive findings, especially in the base. In all included patients, chemiluminescence was visible in the base in varying degrees, even when the primary tumor was not located there, and it was observed in nonradioactive specimens as well. The latter proved that this signal does not originate from ^{68}Ga-PSMA-11. Extensive rinsing with sodium chloride did not make the signal disappear, thus eliminating the effect of radioactive urine and blood contamination, as was initially suggested by Darr et al. (*13*). Our hypothesis is that this signal is chemiluminescence, caused by the use of diathermy. The sudden heat from electrosurgery is known to result in the production of reactive oxygen species (*24*). After a cascade of reactions, decomposition of the molecule occurs, resulting in emission of optical photons. These photons partially overlap with the Cerenkov spectrum (*9*,*13*,*14*). In our institute, diathermy is performed mainly when separating the prostate from the bladder, though it is also used in other areas. Therefore, chemiluminescence is most prevalent at

TABLE 2
Overview of Histopathology and CLI Results from 10 Histopathologic PSMs

Patient no.	Location of PSM on histopathology	LS	SBR on CLI	Gleason score at PSM	Extent of PSM on histopathology (mm)	Extent of PSM on CLI (mm)
1	Apex right	5	13.2	8	3	6.9
2	Apex left	5	5.9	8	4	4.3
8	Base central	3	7.1	10	14	14
	Base left	3	6.1	10	14	12
	Apex right	5	8.7	10	15	12
	Base right	3	6.1	9	10	9.6
10	Base central	3	5.1	8	9.0	6.7
12	Apex posterior/mid prostate	5	2.8	3 + 4 = 7	6.0	6.5
13	Apex left	5	2.9	8	1.0	1.4
14	Apex posterior/mid prostate	5	12.3	10	2.0	12.0

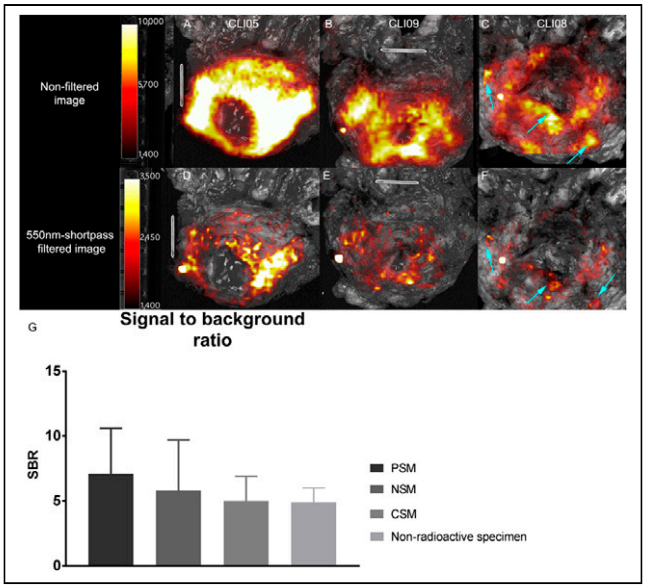

FIGURE 3. CLI images from prostate base in ^{68}Ga-PSMA-11 patients and bar chart showing SBR of CLI and chemiluminescence. (A and B) Unfiltered images of chemiluminescence at base. (D and E) Corresponding 550-nm short-pass filtered images. (C and F) Base of patient 8, who had multiple PSMs at base (arrows). These images show that visual distinction between chemiluminescence and actual PSMs is difficult. (G) Bar chart displaying SBR of chemiluminescence in nonradioactive specimens and that of PSM, NSM, and CSM in patient nonfiltered and filtered images. Average SBR is derived from all patient data, in which lesions on all sides of prostate were included. Note difference in scaling.

the base, explaining why the correspondence between CLI (hot spot, yes or no) and histopathology was only 20% (Fig. 2). Despite the fact that the addition of image interpretation with an LS improved agreement, 4 PSMs at the base were false-negative on CLI with an LS of 3 (Fig. 3C). To facilitate better detectability of PSMs, the need for a method to distinguish between Cerenkov and the diathermy-induced chemiluminescence is eminent.

The mean SBR of the chemiluminescent signal and the mean number of PSM-suspected hot spots on unfiltered images were comparable: 4.9 ± 1.1 and 5.3 ± 2.3, respectively (Fig. 3). In 550-nm filtered images, the SBR of the PSM was larger, at 9.9 ± 5.5, than the chemiluminescent signal, at 4.2 ± 0.3, though they still overlapped. Next, filtered images are more susceptible to noise, resulting in high SBRs. A study by Spinelli found a heat-induced chemiluminescent half-life of 4–6 min in chicken breast tissue (*15*), suggesting a potential distinction between Cerenkov and chemiluminescence based on half-life. However, the half-lives of the 2 signals in prostatic tissue had a large overlap; chemiluminescence half-life was 48 ± 11 min, compared with 68 min for ^{68}Ga. The discrepancy in chemiluminescence half-life compared with the findings of Spinelli may be explained by the differences in tissue composition and methods used to induce thermal damage. A focused ultrasound transducer (60 W) was used by Spinelli, whereas in our institution a monopolar diathermy device (Intuitive) at 40 W was used.

Another solution may be to look for alternative forms of monopolar diathermy that have a lower wattage resulting in less thermal induction and spread (*25*,*26*), such as the PEAK PlasmaBlade (Medtronic). Next, a theoretic method to reduce the presence of free radicals in tissue, thereby preventing lipid peroxidation, might be the use of antioxidants such as vitamin C or E (*27*), or the influence of rapid cooling might be investigated. Whether these solutions are viable requires further investigation, and for clinical use it is of key importance that they not interfere with the surgical outcome or histopathologic evaluation of the specimens.

FAR, an opaque film that largely blocks optical photons while allowing positrons to be detected directly, was used to investigate whether such blocking is less susceptible to chemiluminescence as CLI. The signal originating from ^{68}Ga-PSMA-11–containing areas (tumor and benign) were enhanced approximately 3.2 times, compared with these areas on CLI (Fig. 5; Supplemental Fig. 3), whereas chemiluminescence was reduced to 70%. Although this technique might help to distinguish between ^{68}Ga-PSMA-11 and chemiluminescence, there are some practical drawbacks to consider. First, because the FAR obscures the white-light image, anatomic and spatial information about the specimen is absent. Second, accurate positioning of the FAR onto the specimen proved challenging, and more work is needed to improve ease of use. Third, the FAR does not block all optical photons originating from the chemiluminescence (Fig. 5). Finally, contamination of the scintillator might lead to false-positive hot spots (Fig. 5).

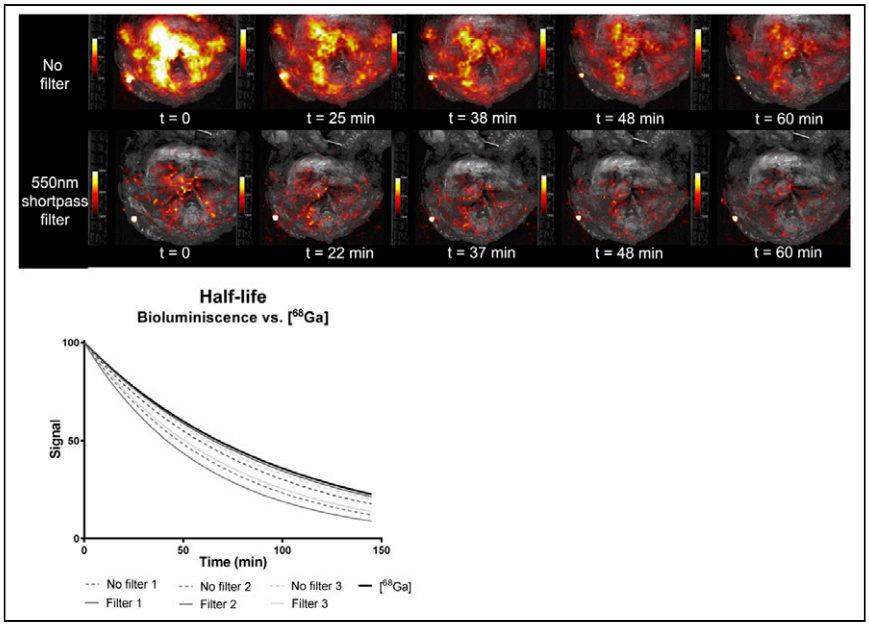

FIGURE 4. Sequential imaging of nonradioactive prostate specimens to determine effect of time on intensity of chemiluminescence signal. Same scaling is used in all images. Graph displays half-life of chemiluminescence in 3 nonradioactive specimens on filtered and nonfiltered images and of ^{68}Ga.

Future Perspectives on CLI

The current histopathologic definition of a PSM, being tumor on ink, is a requirement that currently cannot be met with ^{68}Ga-PSMA CLI. Therefore,

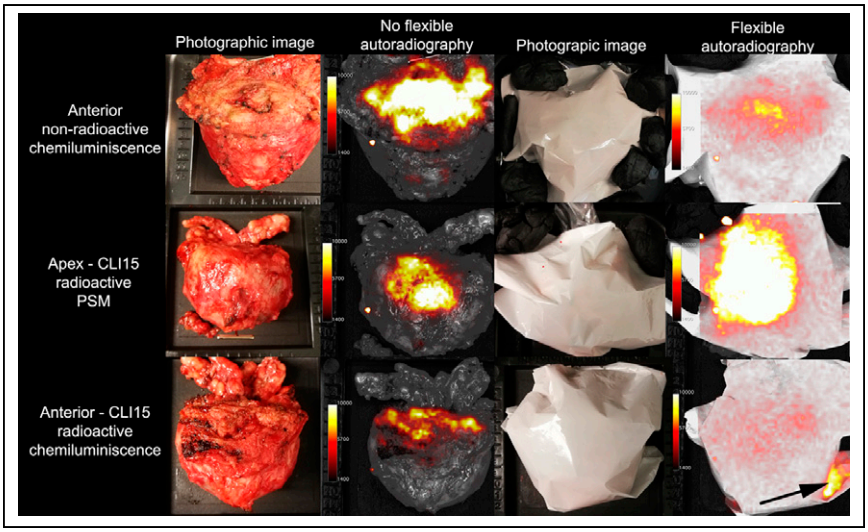

FIGURE 5. FAR images of ^{68}Ga-PSMA-11–containing prostate specimens and nonradioactive prostate specimens to investigate effect of FAR on tumor and chemiluminescent signal levels. FAR reduced chemiluminescence in both nonradioactive (60%) and radioactive specimen (70%) (top and bottom rows). FAR amplified signal originating from tumor (center row). Arrow shows contamination of scintillator. Same scaling is used for all images.

instead of using CLI as a stand-alone technology, our group proposes using CLI as a screening tool combined with NeuroSAFE. By sending, for pathologic examination, only areas that show suggestive hot spots on Cerenkov images instead of the entire neurovascular bundle, the procedure may become far more efficient (Supplemental Fig. 4); 60%–75% of PSMs occur at the apex or posterolateral side of the prostate (*23*,*28*), whereas chemiluminescence occurs especially at the base. When diathermy is used in other prostate areas, surgeons are able to identify these locations visually. Therefore, inclusion of this knowledge during image interpretation may further improve the accuracy of CLI for combined use with NeuroSAFE.

CONCLUSION

CLI of ^{68}Ga-PSMA-11 can be used for margin assessment during prostatectomy. In the current study, agreement between CLI and histopathology was 31%–83% for the entire prostate, depending on the definition of PSM and application of image interpretation using the LS. The best identification of margin status was achieved for cancer infiltrating the outer 1 mm of the specimen on histopathology. The presence of chemiluminescence from diathermy, especially profound in the basal area, hampers accurate image interpretation of CLI. Therefore, ^{68}Ga-PSMA-11 CLI is most applicable to the detection of CSMs and PSMs in the apex and posterolateral side.

DISCLOSURE

Kunal Vyas and Maarten Grootendorst are employees of and have equity interest in Lightpoint Medical Ltd. This research is supported by KWF Kankerbestrijding and Technology Foundation STW, as part of their joint strategic research program "Technology for Oncology" (grant 15175). No other potential conflict of interest relevant to this article was reported.

KEY POINTS

QUESTION: Can CLI be used to detect PSMs intraoperatively in prostate cancer surgery?

PERTINENT FINDINGS: In this clinical trial of 15 patients, CLI was able to detect PSMs and tumor close to the surface (≤1 mm). Still, the presence of diathermy-induced chemiluminescence hampers the application in its current form.

IMPLICATIONS FOR PATIENT CARE: CLI showed potential as an intraoperative method to find tumors close to the surface; however, the influence of a chemiluminescent artifact on the CLI images should be reduced before clinical implementation.

REFERENCES

1. Yossepowitch O, Briganti A, Eastham JA, et al. Positive surgical margins after radical prostatectomy: a systematic review and contemporary update. *Eur Urol.* 2014;65:303–313.
2. Stephenson AJ, Wood DP, Kattan MW, et al. Location, extent and number of positive surgical margins do not improve accuracy of predicting prostate cancer recurrence after radical prostatectomy. *J Urol.* 2009;182:1357–1363.
3. Silberstein JL, Eastham J. Significance and management of positive surgical margins at the time of radical prostatectomy. *Indian J Urol.* 2014;30:423–428.
4. olde Heuvel J, de Wit-van der Veen BJ, Huizing DMV, et al. State-of-the-art intraoperative imaging technologies for prostate margin assessment: a systematic review. *Eur Urol Focus.* 2021;7:733–741.
5. Schlomm T, Tennstedt P, Huxhold C, et al. Neurovascular structure-adjacent frozen-section examination (NeuroSAFE) increases nerve-sparing frequency and reduces positive surgical margins in open and robot-assisted laparoscopic radical prostatectomy: experience after 11,069 consecutive patients. *Eur Urol.* 2012;62:333–340.
6. Dinneen EP, Van Der Slot M, Adasonla K, et al. Intraoperative frozen section for margin evaluation during radical prostatectomy: a systematic review. *Eur Urol Focus.* 2020;6:664–673.
7. van der Slot MA, Bakker MA, Klaver S, et al. Intraoperative assessment and reporting of radical prostatectomy specimens to guide nerve-sparing surgery in prostate cancer patients (NeuroSAFE). *Histopathology.* 2020;77:539–547.
8. Grootendorst MR, Cariati M, Pinder SE, et al. Intraoperative assessment of tumor resection margins in breast-conserving surgery using ^{18}F-FDG Cerenkov luminescence imaging: a first-in-human feasibility study. *J Nucl Med.* 2017;58:891–898.
9. Ciarrocchi E, Belcari N. Cerenkov luminescence imaging: physics principles and potential applications in biomedical sciences. *EJNMMI Phys.* 2017;4:14.
10. Robertson R, Germanos MS, Li C, Mitchell GS, Cherry SR, Silva MD. Optical imaging of Cerenkov light generation from positron-emitting radiotracers. *Phys Med Biol.*2009;54:N355–N365.
11. Tanha K, Pashazadeh AM, Pogue BW. Review of biomedical Čerenkov luminescence imaging applications. *Biomed Opt Express.* 2015;6:3053–3065.
12. Thorek DLJ, Riedl CC, Grimm J. Clinical Cerenkov luminescence imaging of ^{18}F-FDG. *J Nucl Med.* 2014;55:95–98.
13. Darr C, Harke N, Radtke JP, et al. Intraoperative ^{68}gallium-PSMA Cerenkov luminescence imaging for surgical margins in radical prostatectomy: a feasibility study. *J Nucl Med.* 2020;61:1500–1506.
14. olde Heuvel J, de Wit-van der Veen BJ, van der Poel HG, et al. ^{68}Ga-PSMA Cerenkov luminescence imaging in primary prostate cancer: first-in-man series. *Eur J Nucl Med Mol Imaging.* 2020;47:2624–2632
15. Spinelli AE. Weak light emission of soft tissues induced by heating. *J Biomed Opt.* 2018;23:1–5.
16. Boschi F, Basso PR, Corridori I, et al. Weak biophoton emission after laser surgery application in soft tissues: analysis of the optical features. *J Biophotonics.* 2019;12:e201800260.

17. Vyas KN, Grootendorst M, Mertzanidou T, et al. Flexible scintillator autoradiography for tumor margin inspection using ^{18}F-FDG. *Proc. SPIE.* 2018;10478:11.
18. Samaratunga H, Montironi R, True L, et al. International Society of Urological Pathology (ISUP) consensus conference on handling and staging of radical prostatectomy specimens: working group 1—specimen handling. *Mod Pathol.* 2011;24: 6–15.
19. Pukelsheim F. The three sigma rule. *Am Stat.* 1994;48:88–91.
20. Moses WW. Fundamental limits of spatial resolution in PET. *Nucl Instrum Methods Phys Res A.* 2011;648(suppl):S236–S240.
21. Herforth C, Stroup SP, Chen Z, et al. Radical prostatectomy and the effect of close surgical margins: results from the shared equal access regional cancer hospital (SEARCH) database. *BJU Int.* 2018;122:592–598.
22. Izard JP, True LD, May P, et al. Prostate cancer that is within 0.1 mm of the surgical margin of a radical prostatectomy predicts greater likelihood of recurrence. *Am J Surg Pathol.* 2014;38:333–338.
23. Koskas Y, Lannes F, Branger N, et al. Extent of positive surgical margins following radical prostatectomy: impact on biochemical recurrence with long-term follow-up. *BMC Urol.* 2019;19:37.
24. Kobayashi K, Okabe H, Kawano S, Hidaka Y, Hara K. Biophoton emission induced by heat shock. *PLoS One.* 2014;9:e105700.
25. Lyons SD, Law KSK. Laparoscopic vessel sealing technologies. *J Minim Invasive Gynecol.* 2013;20:301–307.
26. Hefermehl LJ, Largo RA, Hermanns T, Poyet C, Sulser T, Eberli D. Lateral temperature spread of monopolar, bipolar and ultrasonic instruments for robot-assisted laparoscopic surgery. *BJU Int.* 2014;114:245–252.
27. Catala A. Lipid peroxidation. In: Repetto M, Semprine J, Boveris A, eds. *Lipid Peroxidation: Chemical Mechanism, Biological Implications and Analytical Determination.* IntechOpen; 2012:3–30.
28. Eastham JA, Kuroiwa K, Ohori M, et al. Prognostic significance of location of positive margins in radical prostatectomy specimens. *Urology.* 2007;70:965–969.